Tsai's calibration applied for close-range hydraulic engineering research

Wei Li
Department of Civil & Environmental Engineering
University of Auckland
Auckland, New Zealand

Trevor Gee
Department of Computer Science
University of Auckland
Auckland, New Zealand

Patrice Delmas
Department of Computer Science
University of Auckland
Auckland, New Zealand

Heide Friedrich
Department of Civil & Environmental Engineering
University of Auckland
Auckland, New Zealand

***Abstract*—Proprietary high-frequency industrial stereo-vision systems can be used for close range applications in dynamic environments. Those systems incorporate faster computation and real-time processing. Alternatively, Tsai's calibration method is well suited for high-frequency applications using non-proprietary stereo-vision systems. In this paper, we study and compare the performance of using low-cost cameras for close range applications in dynamic environments. The camera configurations tested had substantial lens distortion, and we show how the corner detection method can be adjusted to be better suited for our specific application. We show that using Tsai's calibration results in accurate representation of close range objects relevant for hydraulic engineering applications. We discuss in detail the effect of camera to target distance and image coverage for the various camera configurations used in this study. Depth resolution, surface accuracy and efficiency of the acquisition process are used as our recommendation criteria for future application of Tsai's calibration in hydraulic engineering research.**

Keywords—Tsai; calibration; distortion; pipeline

I. INTRODUCTION

Close-range photogrammetry measurement and 3D scene reconstruction are becoming more popular for applications in hydraulic engineering research [1-6]. Consumer-grade cameras, like the Gopro series' cameras, can now be used for the 3D reconstruction of dynamic environments [1] [2], whereas more recently industrial cameras and stereo-vision systems dominated the market [3].

In hydraulic engineering, stereo-vision solutions are used for the investigations of the seafloor mapping [1], the bed evolution [4], and measuring gravel-bed topography [5] [6]. Those applications pre-dominantly use Bouguet's calibration method [7], which is freely available for stereo-photogrammetric solutions, and is based on Zhang's calibration method. Using Bouguet's calibration toolbox allows sub-pixel accuracy. Together with implementing an optimized workflow [8], makes Bouguet's calibration toolbox an important tool to achieve a high-performing non-proprietary calibration and stereo-matching solution in hydraulic research.

However, the majority of the processes we study are highly-dynamic in nature, and thus real-time image capturing and post-processing is becoming more important for using the stereo-vision technique in hydraulic engineering applications. Dynamic maps of river topographies can help parameterize mass, momentum and energy balance equations of the river system [9]. The stereo-vision technique can also be applied for monitoring the morphology of a stream bed with uninterrupted, instantaneous, highly detailed 3D representations [10] [11].

Previously, we used Zhang's calibration method, which requires multiple images (more than 15 pairs) to reach an acceptable sub-pixel accuracy for the re-projection error [8]. For dynamic environments, it is therefore not practical to employ Zhang's calibration method, as whilst acquiring those many image pairs, important information of the dynamic behavior is lost. For our specifically targeted hydraulic engineering applications, such as time-resolved capturing of flow and sediment processes in a laboratory flume or in the field, the interaction between flowing water and moving sediment increases the difficulty of the stereo-vision application.

Tsai's calibration method, requiring only one image pair, seems a more suitable calibration method for studying those dynamic hydraulic applications. Previously we showed there is a trade-off between accuracy and practical efficiency [14]. Tsai's calibration method [12] is using a non-planar target, and thus 'instant' calibration can be achieved with only one image pair. Due to our specific hydraulic engineering application requirements, lens distortion is an important factor. A simple distortion model is recommended for most general stereo-vision applications [12] [13]. Taking distortion into account for different camera models, we study if a stereo-vision pipeline

978-1-5090-0357-0/15/$31.00 ©2015 IEEE

based on Tsai's calibration method could provide an acceptable accuracy for our future applications.

II. STEREO-VISION PIPELINE

Figure 1 shows a general stereo-vision pipeline. After a stereo setup has been designed, image pairs of the calibration target, such as a chequerboard, are acquired to compute the intrinsic and extrinsic parameters of the stereo-camera configuration. A corner detection algorithm is used for calibration. Thereafter, calibration accuracy can be evaluated by assessing the re-projection and rectification errors. Those values provide a general idea of the successful implementation of a stereo-vision pipeline. For the image pairs of the studied dynamic behavior, images will be undistorted and rectified, before stereo matching provides a depth map, with subsequent 3D reconstruction as a Digital Elevation Model (DEM).

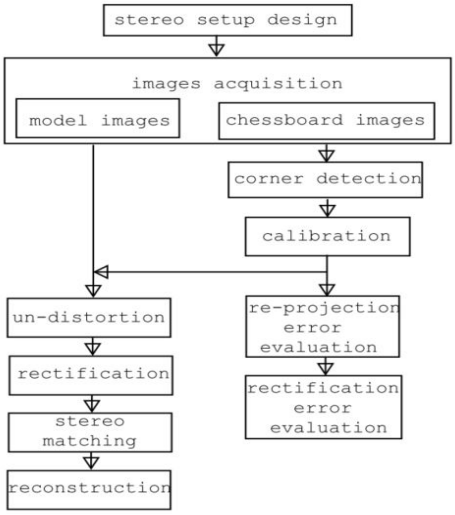

Fig. 1. General stereo-vision pipeline.

A. Stereo-setup design

Theoretical stereo-vision accuracy largely depends on the setup configuration, taking into account the specification of the cameras and the position of the two cameras. Practically, this means that a suitable setup meets design demands, such as camera to object distance, baseline, object resolution and depth resolution and general acquisition efficiency. Figure 2 shows a frontal parallel stereo-vision setup.

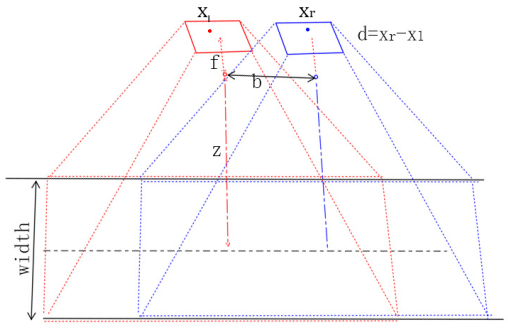

Fig. 2. Stereo-vision setup.

Using the stereo camera specifications such as pixel size $delta$, initial focus length f, distance z, baseline b and the point disparity d, computed from one world point (x_w, y_w, z_w) and projected to the left and right images, (x_l, y_l) and (x_r, y_r), a set of parameter representing the setup can be computed for evaluation. Amongst them, surface accuracy, S_A, and depth resolution, D_A, are the two most commonly used ones. The following equations are used

$$S_A = \left(\frac{z \times delta}{f}\right)^2 \quad (1)$$

$$D_A = f \times \frac{b}{d(d+1)} \quad (2)$$

The depth resolution, D_A, is critical for the design of setup, and generally one can say that designing for a closer distance results in a more accurate measurement. This statement does not take lens distortion into account. For cameras with high lens distortion, a closer camera to object distance actually can decrease the reconstructed DEM accuracy. Figure 3 shows how a camera to object distance adjustment affects on the measured target, when taking into account distortion.

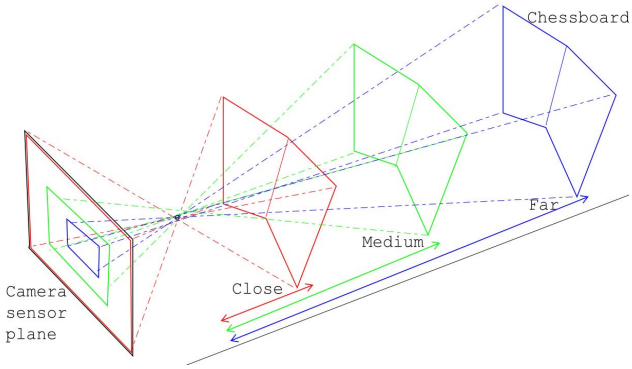

Fig. 3. Effect of changes in target to camera distance for Tsai's calibration.

In the following, we introduce in more detail parts of the stereo-vision pipeline that are used to undistort, rectify and stereo match an object with sufficient theoretical accuracy, before outlining our calibration accuracy evaluation.

B. Un-distortion

We use one inverse mapping method [15] based on Brown's distortion model, which determines a distorted point's corresponding undistorted point to remap the distorted image to the undistorted image.

C. Rectification

Stereo-image rectification is based on a frontal parallel arrangement of cameras, using epipolar geometry. Fusiello's [16] method is used to compute the new projection matrixes to realize the rectification important for stereo matching.

D. Stereo matching

The stereo dynamic programming algorithm developed by Nguyen [17] is used, thus reducing our previously high processing cost. The stereo matching method has been previously confirmed to be suitable for hydraulic applications

[8]. With the depth map computed, a 3D reconstruction can then be undertaken.

E. Accuracy evaluation

The accuracy of the calibration is usually evaluated by the projection error. Usually, three kinds of errors [12] are used to evaluate the accuracy of calibration: re-projection error, sensor plane error and projection error. The re-projection error, ε_{pe}, being the discrepancy between the observed pixel coordinate, (x_{pi}, y_{pi}), and the estimated pixel coordinate, $(\hat{x}_{pi}, \hat{y}_{pi})$, by projecting the measured world coordinate of the model to the distorted camera plane, is commonly used in practical applications. Given the total number of points, n, the re-projection error can be computed by formula (3), and the unit is in pixel.

$$\varepsilon_{pe} = \frac{\sum_{i=1}^{n} \sqrt{(\hat{x}_{pi} - x_{pi})^2 + (\hat{y}_{pi} - y_{pi})^2}}{n} \quad (3)$$

The rectification error, ε_{re}, is usually used to evaluate whether left and right images are exactly aligned in the frontal parallel configuration, which is measured by the y-axis discrepancy between the left pixel coordinate, (x_{li}, y_{li}) and (x_{ri}, y_{ri}) via formula (4) in pixel unit

$$\varepsilon_{re} = \frac{\sum_{i=1}^{n} (|y_{ri} - y_{li}|)}{n} \quad (4)$$

III. METHODOLOGIES

A. Experimental methodology

The objective of the project is to develop a high-frequency, high-resolution stereo-vision system for hydraulic engineering research. We therefore undertook all image acquisitions in the hydraulic environment. We conducted our studies in a 19 m long, 0.45 m wide and 0.5 m deep hydraulic flume in the Hydraulic Engineering Laboratory of the University of Auckland. Measurements in a hydraulic flume are restrained by the flume width – therefore our ideal camera to target distance should allow for the acquired image pairs to cover the flume width at the flume bed. The cameras' common field of view (CFoV) should therefore cover the width of the flume, whilst still acquiring images with the highest resolution possible, lens depended.

For our study we use three pairs of cameras for our experiments, namely Gopro Hero2 and Gopro Hero3 cameras and Basler acA2000-50gc industrial cameras. For the Basler cameras, two pairs of lenses, with 9 mm and 25 mm focus length, are used. We call those Basler camera configurations Basler1 (with 9 mm lens) and Basler2 (with 25 mm lens) from now on. Gopro cameras are popular consumer-grade cameras with large field of view (FoV). Due to their large FoV, Gopro cameras display high distortion. Basler cameras are traditionally industrial-grade cameras. The cameras come with Basler's acquisition system, which provides comprehensive capturing operations from exposure setting to raw data de-mosaicking. Using the Basler cameras with the 9 mm and 25 mm lenses results in less distorted image pairs than the ones captured with the Gopro cameras, with almost no distortion visible for the 25 mm lens.

3D housings are used for both Gopro Hero2 and Gopro Hero3 cameras, thus allowing synchronized image capturing. For the present study, images and not videos are captured for the Gopro cameras. Gopro Hero2 and Gopro Hero3 image resolution was set to 3840*2880 and 4000*3000 pixels, respectively. For both used Gopro 3D housings, the baseline is around 35 mm.

For the used Basler cameras, a maximum color image resolution of 2046*1086 at 25 frames per second can be achieved. If using grey image setting, the acquisition frame rate can be doubled to 50 frames per second. Frames are stored directly into the computer's hardware drive, instead of volume limited SD card as for Gopro cameras. Thus, theoretically, the operation of the Basler cameras is the more flexible and potentially more suitable for high-frequency stereo-vision application in hydraulic engineering application.

For now, our acquisition takes place above water. In future, Gopro's SD card storage might become an advantage when we move to underwater applications, as together with the waterproof 3D housing, it allows straightforward deployment in the water. Thus, we continue to test both Gopro and Basler cameras for the near future, due to each of their advantages for certain hydraulic engineering applications. Relevant pipeline camera specifications are shown in table I.

TABLE I. CAMERA AND STEREO-DESIGN PARAMETERS

	Camera Type			
	Gopro Hero2	***Gopro Hero3***	***Basler1***	***Basler2***
Sensor size (mm)	5.37×4.04	6.17×4.55	8.8×6.6	
Resolution (px)	3840×2880	4000×3000	2046×1086	
Pixel size (μm)	1.4	1.55	5.5	
Focus (mm)	2.85	2.96	9	25
Baseline (mm)	35	35	200	
$\kappa 1$ (mm^{-2})	0.066	0.057	0.0025	0.00018
z (mm)	320	296	623	1730
S_A (px/mm^2)	40.47	41.62	6.90	6.90
D_A (mm)	1.43	1.31	1.18	3.29

The setup of the Basler cameras in the hydraulic flume and the experimental lighting environment are shown in figure 4. The lighting used were two 1 m long neon lights, installed next to the transparent sides of the flume, along the test section of the flume. A frame, to fix the vertical position of the cameras, allows to adjust the height of different cameras to the flume bed. Our working vertical height range is 250 mm to 2200 mm.

Fig. 4. Experimental setup in the hydraulic flume with Tsai calibration target (left) and lighting setup with two 1 m long neon lights placed at both sides of the flume (right).

Figure 5 shows our used 3D chequerboard Tsai calibration target, which is 450 mm wide. Thus, the target can be placed into the 450 mm wide flume. The chequerboard is printed on paper with 19 horizontal squares and 15 vertical squares, with square sizes of 30 mm, printed by a laser printer with an accuracy of 20 μm. We use a 'hemisphere model' [8] made of 9 ping pong balls, with 40 mm diameter, to evaluate the accuracy of different setups after calibration, rectification and stereo matching. Small colored sand particles are placed on the surface of the 'hemisphere model' to increase the success of stereo matching.

Fig. 5. Calibration target and the 'hemisphere model'.

B. Detailed corner detection evaluation due to lens distortion

For the cameras we used, distortion coefficients based on Tsai's distortion model are provided by the camera manufactures. Care must be taken, as variations to the distortion parameters can be introduced by variations of the focus length and κ1. For our experiments, distorted image pairs taken with Gopro Hero2 and Gopro Hero3 cameras, could not be undistorted with a freely available OpenCV's chequerboard corner detection method, and we used our previously developed corner detection method [14]. We compare the corner detection results, and the mean error and standard deviation of the absolute difference in pixel unit are shown in table II. The analysis is based on a set of 10 planar chequerboard images taken with the various camera configurations. Since there is no ground truth for corner coordinates, we use the absolute difference of the corner coordinates, extracted independently with the two corner detection methods from the images, to evaluate the difference of the two methods.

TABLE II. CORNER COORDINATE ABSOLUTE DIFFERENCE (PIXEL) BETWEEN OPENCV'S AND OURCORNER DETECTION METHOD

	Camera Type			
	Gopro Hero2	***Gopro Hero3***	***Basler1***	***Basler2***
Error	0.116±0.051	0.117±0.059	0.082±0.034	0.075±0.032

C. Evaluations

Due to the extensive lens distortion for the cameras tested, we studied the effect of close 'C', medium 'M' and far 'F' camera to object distance for Tsai's calibration method. This also allowed a second evaluation of studying the effect of image coverage on the calibration results.

*1) Effect of distance to object on calibration: The stereo-*vision pipeline based on Tsai was conducted *for* the four camera configurations independently. Cameras were set up to allow coverage of the whol*e flume width for each configuration.* Table I shows values of the theoretical accuracy, such as surface accuracy, S_A, and depth resolution, D_A, based on the ideal pin-hole camera model at the distance, z, for the stereo setup when the whole width of the flume is covered.

Although theoretically a closer distance to object should

TABLE II. CALIBRATION RESULTS OF FOCUS LENGTH, K1 BASED ON DISTANCE

	Camera Type											
	Gopro Hero2			***Gopro Hero3***			***Basler1***			***Basler2***		
	z(mm)	***f(mm)***	***κ1 (mm^{-2})***	***z(mm)***	***f(mm)***	***κ1 (mm^{-2})***	***z(mm)***	***f(mm)***	***κ1 (mm^{-2})1***	***z(mm)***	***f(mm)***	***κ1 (mm^{-2})1***
Whole	C=381	3.02	0.066	C=367	2.70	0.057	C=860	9.37	0.0025	C=2000	26.81	0.00018
	M=468	2.89	0.060	M=502	2.75	0.046	M=1107	9.23	0.0021	M=2200	26.30	0.00017
	F=624	2.85	0.056	F=665	2.76	0.041	F=1531	9.12	0.0019	N/A	N/A	N/A
Centre	C=381	2.87	0.056	C=367	2.71	0.042	C=860	9.17	0.0020	C=2000	26.52	0.00017
	M=468	2.88	0.057	M=502	2.72	0.042	M=1107	9.15	0.0019	M=2200	26.23	0.00017

TABLE IV. RE-PROJECTION ERROR (PIXELS) BASED ON WHOLE CORNERS AND CENTRE CORNERS (LARGEST ERRORS ARE IN GREY BACKGROUND AND BASLER2 AT F DISTANCE IS NOT AVAILABLE)

ε_{pe}(pixel)		**Camera Type**							
		Gopro Hero2		***Gopro Hero3***		***Basler1***		***Basler2***	
		Left	***Right***	***Left***	***Right***	***Left***	***Right***	***Left***	***Right***
Whole	C	29.10±54.45	22.21±48.37	20.39±49.41	21.70±51.60	0.62±0.86	0.84±0.84	0.58±0.31	0.45±0.29
	M	3.39±2.02	2.56±1.72	1.19±0.94	2.39±1.74	0.47±0.28	0.48±0.29	0.48±0.29	0.39±0.25
	F	1.25±0.69	0.91±0.73	0.73±0.59	1.15±0.87	0.41±0.26	0.39±0.23	N/A	N/A
Centre	C	1.31±0.77	0.94±0.52	0.73±0.63	1.39±1.06	0.50±0.31	0.33±0.20	0.54±0.36	0.44±0.24
	M	1.36±0.71	0.90±0.64	0.68±0.57	1.20±0.62	0.44±0.25	0.37±0.23	0.48±0.29	0.39±0.25

allow more accurate depth resolution, in our case the existence of substantial lens distortion can potentially decrease the calibration accuracy, as well as having a detrimental impact on the effective CFoV. Alternatively, there is another option of only using the information in the centre of the image pairs to reconstruct a stereo scene. This will reduce though the sampling resolution, as a large amount of the captured image is wasted. Therefore, optimization has to take place between accurate representation of the 3D scene and achievable surface resolution and depth accuracy.

For the three distances we studied, 'C', 'M' and 'F', radial distortion increases at the square order with the distance to the image centre. Thus the closer to the image centre, the less distortion will occur. We chose 'C', 'M' and 'F' to reflect the full coverage of the calibration target, and 2/3 and 1/3 coverage, as is shown in figure 6. The whole chequerboard is covered for 'C', but as figure 6 shows, contains severe distortion. Increasing the camera to object distance is reducing the distortion in the images.

2) Effect of image coverage on calibration: For cases 'C' and 'M' we also studied the effect of using only the central part of chequerboard corners for Tsai' calibration method. *We wanted to see if the close distance, which is affected by severe distortion, actually still provides accurate 3D reconstruction if only the 'centre' of the image, and thus calibration target, is used for further analysis, compared to the 'whole' calibration target.* Figure 6 shows our definition of 'centre' and 'whole' image areas, with images captured at 'C' and 'M" distance covering 13×7 squares for the 'centre' case and 15×11 squares for the 'whole' case. Whereas for the 'F' case, we only studied the 'whole' scenario, taking into account all 19×15 squares.

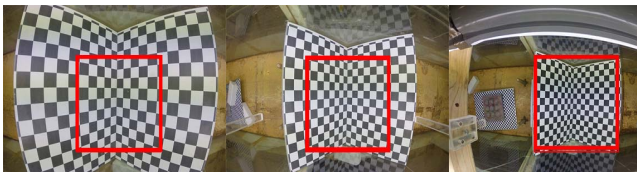

Fig. 6. The choice of target centre area.

IV. RESULTS & DISCUSSION

The distance, focus length and κ1 results for the left camera of every setup are shown in table III.

A. Re-projection error

The re-projection error is presented in table IV. Because the focus length is different for each camera configuration, the three camera to object distances vary between configurations, as the main objective was to cover the flume width at the flume bed. That means for case, 'C','M' and 'F' – the actual camera to object distance is different. Since our frame that supports the stereo-vision setup allows only a maximum distance of 2200 mm, we were not able to set up an 'F' case for the Basler2 camera configuration.

The re-projection error is shown for each camera configuration in table IV. It shows that both, Basler1 and Basler2 configurations, have an acceptable theoretical performance. For the Gopro configurations, the large lens distortion does provide challenges, however, by increasing the camera to object distance, an acceptable performance can be achieved, albeit by reducing the sampling resolution.

B. Rectification error

The rectification error is presented in table V. It shows that using only the centre squares for Gopro Hero2 and Gopro Hero3, calibration accuracy can be improved substantially.

TABLE V. RECTIFICATION ERROR (PIXELS) BASED ON WHOLE CORNERS AND CENTRE CORNERS CALIBRATION (ERRORS LARGER THAN 1 PIXEL ARE IN GREY)

ε_{re}(pixel)		Camera Type			
		Gopro Hero2	***Gopro Hero3***	***Basler1***	***Basler2***
Whole	C	4.99±4.31	1.99±1.65	1.05±1.24	0.52±0.18
	M	2.78±2.10	1.09±0.83	0.63±0.22	0.47±0.16
	F	0.91±0.73	0.73±0.56	0.48±0.43	0.43±0.17
Centre	C	1.12±0.84	0.52±0.42	0.47±0.18	0.32±0.29
	M	0.79±0.60	0.62±0.51	0.43±0.34	0.34±0.20

C. Depth map

The 'hemisphere model' is used to visually study the performance of the various camera configurations. This is achieved by computing the depth map based on the calibration results. Figure 7 shows the stereo matching results for each camera configuration, for both, the 'whole' and 'centre' calibration cases. One can see that generally more noise, and thus stereo-matching errors, are visible in the left image, which is the one for which the 'whole' calibration area was used.

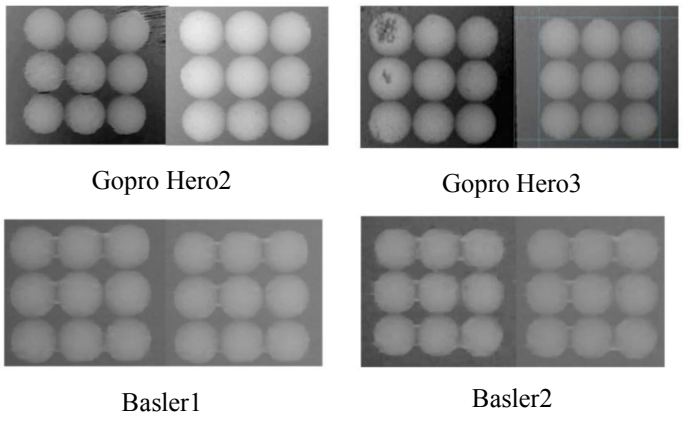

Fig. 7. Depth map results for 'whole' and 'centre' calibration targed case for each tested camera configuration 'Whole' is the left image of the pair, and 'centre' is the right image of the pair.

D. DEM reconstruction

Based on the stereo matching results, the measured 'hemisphere model' can be reconstructed and then further converted to DEMs, as shown in figure 8.

It is clearly seen that the DEM quality of the Basler2 configuration, due its substantially lower theoretical depth accuracy (see table I), lacks behind the other tested configurations. By using the 'centre' calibration, Gopro Hero2 and Gopro Hero3 do actually provide acceptable DEMs, which

is very satisfying. The Basler1 configuration is not performing as well as the Gopro configurations, but still outperforms the Basler2 configurations due its higher theoretical depth accuracy.

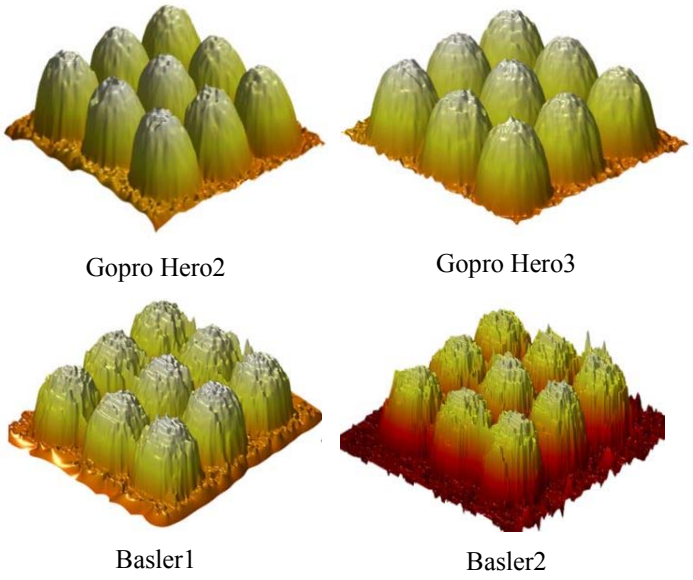

Fig. 8. The reconstructed DEMs based on the 'centre' calibration case for 'C' camera to object distance.

V. CONCLUSION

Tsai's calibration method has the potential to be used for real-time stereo-vision application in hydraulic engineering research due to its efficient single image pair calibration workflow. For the Basler configurations we tested, which are prone to partly severe lens distortion, we show that by designing the stereo setup to take into account camera to object distance and image coverage for calibration, the accuracy achievable can be characterized by a sub-pixel re-projection error. The depth map and reconstructed DEM visually confirm the quality of the results. Therefore, we recommend to continue work on implementing Tsai's calibration method for our future hydraulic engineering stereo-vision studies.

For the studied Gopro cameras, the result is slightly different. Using Tsai's calibration results in both, higher re-projection error and rectification error, with subsequent poor depth map and 3D reconstruction accuracy. However, we show that by using only the center corners of the calibration image pairs, we can reduce the re-projection and rectification errors substantially. Thus allowing accurate results, although at less resolution than what the cameras would be able to achieve, as only part of the original image pair is used as a region of interest.

ACKNOWLEDGMENT

The study was partly funded by the Marsden Fund (Grant No. UOA1412), administered by the Royal Society of New Zealand.

REFERENCES

[1] V. E. Schmidt and Y. Rzhanov, "Measurement of micro-bathymetry witha gopro u]nderwater stereo camera pair," in Oceans, 2012. IEEE, 2012,pp. 1–6.

[2] Y. H. Chan, M. Nguyen, A. Gastelum, S. Yang, R. Gong, N. Liu, P. Delmas, G. Gimel'farb, S. Bertin, and H. Friedrich, "The ngongotaha river udps experiment: low-cost underwater dynamic stereo photogrammetry," in Proceedings of the 27th Conference on Image and Vision ComputingNew Zealand. ACM, 2012, pp. 412–417.

[3] S. Lane, J. Chandler, and K. Porfiri, "Monitoring river channel and flume surfaces with digital photogrammetry," Journal of Hydraulic Engineering, vol. 127, no. 10, pp. 871–877, 2001.

[4] E. Foti, I. C. Rabionet, A. Marini, R. E. Musumeci, and A. Sánchez-Arcilla, "Experimental investigations of the bed evolution in wave flumes: Performance of 2d and 3d optical systems," Coastal Engineering, vol. 58, no. 7, pp. 606–622, 2011.

[5] S. Bertin, H. Friedrich, P. Delmas, and E. Chan, "The use of close-range digital stereo-photogrammetry to measure gravel-bed topography in a laboratory environment," in Proceedings of the 35th IAHR Congress, Chengdu, China, 2013.

[6] S. Bertin, and H. Friedrich, "Measurement of gravel-bed topography: an evaluation study applying statistical roughness analysis." *Journal of Hydraulic Engineering*, vol. 140, no. 3, pp.269–279, 2014.

[7] J.-Y. Bouguet, "Camera calibration toolbox for matlab," 2004.

[8] S. Bertin, H. Friedrich, P. Delmas, E. Chan, and G. Gimelfarb, "Digital stereo photogrammetry for grain-scale monitoring of fluvial surfaces: Error evaluation and workflow optimisation," ISPRS Journal of Photogrammetry and Remote Sensing, vol. 101, pp. 193–208, 2015.

[9] J. H. Chandler, E. Ferreira, R. Wackrow, and K. Shiono, "Water surface and velocity measurement-river and flume," 2014.

[10] P. P. Bouratsis, P. Diplas, C. L. Dancey, and N. Apsilidis, "High-resolution 3-d monitoring of evolving sediment beds," Water Resources Research, vol. 49, no. 2, pp. 977–992, 2013.

[11] M. Stojic, J. Chandler, P. Ashmore, and J. Luce, "The assessment of sediment transport rates by automated digital photogrammetry," Photogrammetric Engineering and Remote Sensing, vol. 64, no. 5, pp. 387–395, 1998.

[12] R. Y. Tsai, "A versatile camera calibration technique for high-accuracy 3d machine vision metrology using off-the-shelf tv cameras and lenses," Robotics and Automation, IEEE Journal of, vol. 3, no. 4, pp. 323–344, 1987.

[13] W. Sun and J. R. Cooperstock, "An empirical evaluation of factors influencing camera calibration accuracy using three publicly available techniques," Machine Vision and Applications, vol. 17, no. 1, pp. 51–67, 2006.

[14] W. Li, T. Gee, H. Friedrich, and P. Delmas, "A practical comparison between zhang's and tsai's calibration approaches," in Proceedings of the 29th International Conference on Image and Vision Computing New Zealand. ACM, 2014, p. 166.

[15] J. Park, S.-C. Byun, and B.-U. Lee, "Lens distortion correction using ideal image coordinates," Consumer Electronics, IEEE Transactions on, vol. 55, no. 3, pp. 987–991, 2009.

[16] A. Fusiello, E. Trucco, and A. Verri, "A compact algorithm for rectification of stereo pairs," Machine Vision and Applications, vol. 12, no. 1, pp. 16–22, 2000.

[17] M. Nguyen, G. G. Farb, and P. Delmas, "Web-based on-line computational stereo vision," in *Image and Vision Computing New Zealand, 2008*. IVCNZ 2008. 23rd International Conference. IEEE, 2008, pp. 1–6